Journal of Computer Science and Electrical Engineering
Print ISSN: 2663-1938
Online ISSN: 2663-1946
DOI: https://doi.org/10.61784/jcsee3147

SIMULATION STUDY OF SPMSM VECTOR CONTROL BASED ON FINITE ELEMENT PARAMETER VERIFICATION AND PARAMETER-MATCHED PI TUNING

ShengYuan Ren*,#, HongYang Xiao#
School of Electrical Engineering, Shenyang University of Technology, Shenyang 110870, Liaoning, China.
#*These authors contributed equally.*
**Corresponding Author: ShengYuan Ren*

Abstract: This study develops a traceable RMxprt/Maxwell–Simulink workflow that links finite-element parameter verification with parameter-matched PI tuning for a surface-mounted permanent magnet synchronous motor (SPMSM). A 1.5 kW, 4-pole, 24-slot motor is first examined at the rated point, and its flux density, no-load back electromotive force, dq-axis inductance, and cogging-torque characteristics are checked. The verified control parameters, Rs=2.85 Ω, Ld=Lq=8.2 mH, ψf=0.32 Wb, and J=0.0012 kg·m², are then transferred to a discrete dq-axis vector-control model. Manual PI, parameter-matched PI, and locally optimized PI schemes are compared under the same startup, load-step, sampling, and limiting conditions. Parameter matching reduces the speed drop from 191.40 to 111.11 r/min and the recovery time from 0.01354 to 0.00766 s; local optimization further reduces them to 95.14 r/min and 0.00568 s. Parameter-perturbation tests for resistance, inductance, flux linkage, and inertia show that the matched controller preserves stronger disturbance rejection within the tested range. The proposed workflow provides a reproducible connection among motor parameters, controller gains, and closed-loop dynamic performance.
Keywords: Surface-mounted permanent magnet synchronous motor, Finite element parameter check; Parameter matching PI; Vector control; Local gain sweep; Joint simulation

1 INTRODUCTION

Surface-mounted permanent magnet synchronous motors (SPMSMs) are widely used in industrial servo drives, computer numerical control equipment, robots, electric actuators, and electric vehicles because they combine high efficiency, high torque density, compact construction, and rapid dynamic response. In a surface-mounted topology, the d- and q-axis inductances are nearly equal, so id=0 field-oriented control is commonly adopted below rated speed and electromagnetic torque is regulated mainly through the q-axis current. Nevertheless, practical speed-control quality still depends on controller structure, motor-parameter accuracy, sampling implementation, voltage and current limits, and external disturbances [1]. Conventional SPMSM studies generally follow a sequence of dq-axis modeling, cascaded current and speed loops, PI gain selection, and MATLAB/Simulink verification. Although this route is mature, gains are often obtained through engineering experience or repeated trial and error, which can provide stable operation at a nominal point without establishing a transparent relationship between electrical parameters and closed-loop bandwidth.

Recent work has therefore explored parameter-based gain initialization and automatic refinement to improve transient response and reduce manual tuning [2]. Disturbance-rejection control combined with parameter identification also shows that errors in stator resistance, dq-axis inductance, and permanent-magnet flux linkage can degrade current tracking, torque production, and robustness [3,4]. Finite-element analysis provides a complementary physical basis because RMxprt and Maxwell models can verify the rated operating point and reveal magnetic-flux distribution, no-load back electromotive force, inductance variation, saturation, and cogging-torque characteristics that are simplified in a linear dq model [5]. However, electromagnetic and control simulations are frequently presented as parallel analyses: finite-element results demonstrate motor-body feasibility, while PI gains remain independently tuned. If the parameters entering the controller formulas are not identified explicitly, the joint-simulation process is difficult to reproduce and discrepancies between control-model inputs and curve-derived values may be overlooked.

Parameter uncertainty is equally important in predictive and deadbeat PMSM control. Studies report that inaccurate resistance, inductance, and flux linkage deteriorate current prediction and disturbance response, whereas parameter identification, compensation, and online updating improve robustness [6-8]. A meaningful PI comparison should therefore use identical operating conditions, sampling periods, limiter settings, and load profiles, and should evaluate startup, load application, unloading, current tracking, recovery, and parameter perturbations. To address these requirements, this paper establishes a traceable workflow comprising rated-point verification, finite-element characteristic checking, parameter-matched PI calculation, closed-loop comparison, perturbation testing, and local gain refinement. A 1.5 kW, 4-pole, 24-slot SPMSM is evaluated in RMxprt/Maxwell 2D, and the selected parameters are transferred to a discrete dq-axis Simulink model. Manual PI, parameter-matched PI, and matched PI with local optimization are compared under unified conditions. The contribution is a reproducible connection between motor parameters, gain selection, and measurable speed, torque, and current responses, with clear boundaries for finite-element checking and average-value simulation.

2 MOTOR BODY PARAMETERS AND FINITE ELEMENT CALIBRATION

2.1 Motor Rated Parameters and Structural Parameters

The research object is a 1.5 kW SPMSM rated at 380 V, 50 Hz, and 1500 r/min. Rated torque is calculated from power and speed and is used to define the load step and q-axis current requirement.

$$T_N = 9550\frac{P_N}{n_N} = 9550\times\frac{1.5}{1500} = 9.55N\cdot m \quad 1 \tag{1}$$

The synchronous speed is determined by the power frequency and the number of pole pairs.

$$n_s = 60\frac{f}{p} \quad 2 \tag{2}$$

For fN=50 Hz and nN=1500 r/min, p=2, corresponding to four poles. The AEDT geometry is retained to isolate controller effects: stator diameters 130/82 mm, air gap 0.5 mm, core length 90 mm, and 24 slots. Table 1 summarizes the model.

Table 1 Motor Body and Control Modeling Parameters

Parameter	Symbol	Value	Use
Rated power	PN	1.5 kW	Research object power level
Rated speed	nN	1500 r/min	Speed reference
Rated torque	TN	9.55 N·m	Load disturbance amplitude
Pole pairs	p	2	Electrical angular velocity and torque equation
Stator outer diameter/inner diameter	Dso/Dsi	130/82 mm	Finite element geometry
Air-gap length	δ	0.5 mm	Magnetic density and inductance
Core length	Lstk	90 mm	Torque capability
Stator phase resistance	Rs	2.85 Ω	Current-loop parameter
d/q axis inductance	Ld/Lq	8.2 mH	Control-model value
Permanent magnet flux link	ψf	0.32 Wb	Torque coefficient
Moment of inertia	J	0.0012 kg·m²	Speed loop Parameters
viscous friction coefficient	B	0.0008 N·m·s/rad	Mechanical model
DC bus voltage	Vdc	540 V	SVPWM voltage limiting

2.2 RMxprt/Maxwell Rated Point and Magnetic Field Calibration

RMxprt verifies the rated point, while Maxwell 2D checks flux density, back-EMF, inductance, and cogging torque; neither replaces closed-loop control evaluation.

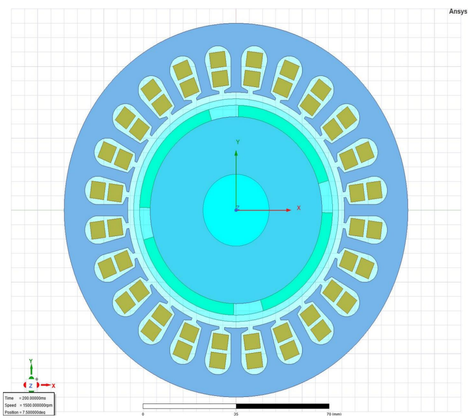

Figure 1 SPMSM Maxwell 2D finite element model

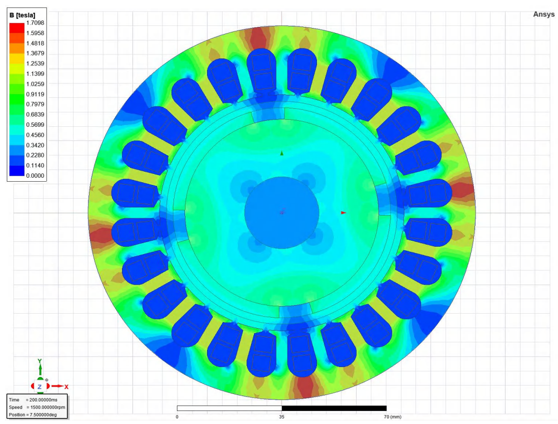

Figure 2 SPMSM Magnetic Flux Density Distribution under No-load Condition

Figures 1 and 2 show the 4-pole, 24-slot surface-magnet model and expected four-pole flux periodicity, confirming magnetic-circuit plausibility rather than PI performance.
Table 2 confirms that output power, speed, and torque match the design targets. Copper loss exceeds iron loss at the rated point; controller dynamics are evaluated separately in Simulink.

Table 2 RMxprt rated point check results

Index	Value	Description
Output power	Approximately 1.501 kW	Basically consistent with the 1.5 kW target
Rated speed	1500 r/min	Match the synchronous speed
Rated torque	Approximately 9.557 N·m	Close to the calculation result of equation (1)
Phase current effective value	Approximately 6.74 A	Used for rated point current verification
efficiency	Approximately 87.02%	RMxprt rated point calculated value
Copper consumption	Approximately 213.6 W	One of the main loss items
iron consumption	Approximately 10.4 W	Rated point iron loss estimate

2.3 Maxwell Key Electromagnetic Parameters and Control Purposes

The no-load back-EMF is used to check ψf. From the fundamental RMS value E1 and electrical angular velocity ωe, ψf is estimated by Equation (3); ψf=0.32 Wb is retained as the control reference.

$$\psi_f = \frac{E_1}{\omega_e} \tag{3}$$

Because the Maxwell fundamental has not been exported, Figure 3 supports only a consistency check and no new quantitative result is claimed.

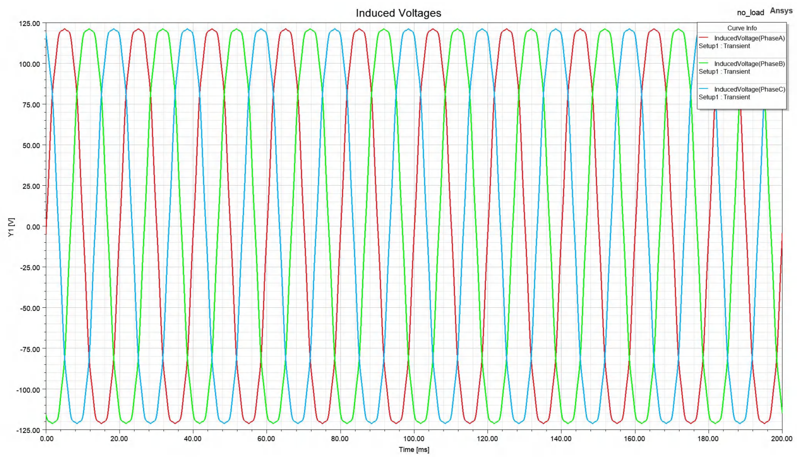

Figure 3 No-load Three-phase Electromotive Force Waveform

Figure 4 shows zero-current cogging torque; its peak-to-peak ratio indicates structural ripple but not the loaded torque response.

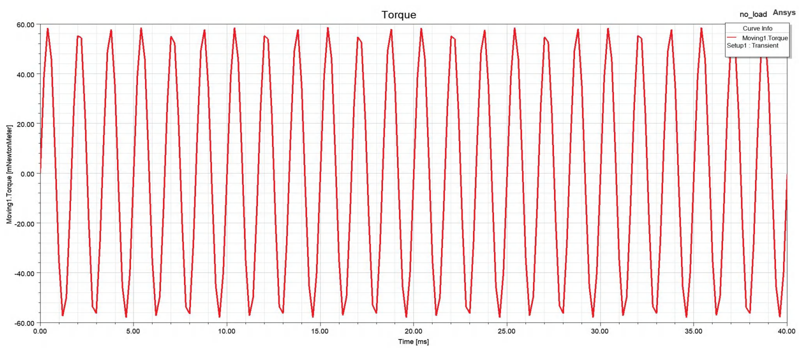

Figure 4 No-load Cogging Torque Waveform

$$k_{\text{cog}} = \frac{T_{\text{cog,max}} - T_{\text{cog,min}}}{T_N} \times 100\% \tag{4}$$

Figure 5 confirms weak saliency. Table 3 therefore separates PI-calculation inductances from approximate Maxwell check values.

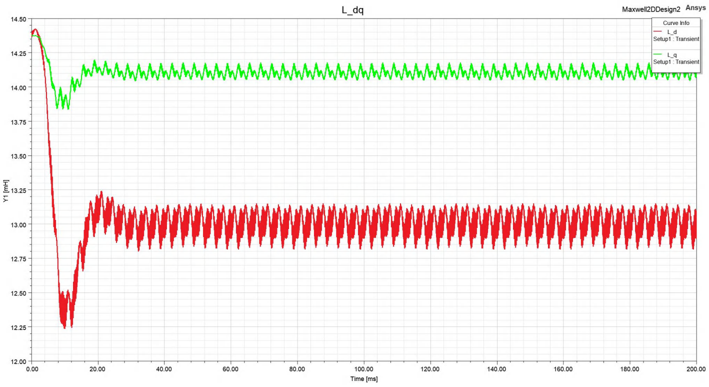

Figure 5 Finite Element Calculation Results of dq-axis Inductance

Table 3 Maxwell Parameter Calibration and Usage Instructions

Parameter	result	Source and description
Permanent magnet flux linkage ψf	0.32 Wb	Control model reference value; continue to check based on the no-load back electromotive force fundamental wave
d-axis inductance Ld	8.2 mH; about 13.0 mH	The former is used for PI calculation; the latter is an approximate Maxwell check value.
q-axis inductance Lq	8.2 mH; about 14.1 mH	The former is used for PI calculation; the latter is an approximate Maxwell check value.
No-load cogging torque	qualitative observation	Qualitative motor-body cogging trend only; no closed-loop performance comparison.
Cogging torque/rated torque	No quantitative conclusions have been drawn	A numerical value requires export and calculation from Maxwell data.

3 MATHEMATICAL MODEL AND PARAMETER MATCHING PI TUNING

3.1 SPMSM dq Mathematical Model

Three-phase PMSM voltages and currents are AC quantities and are therefore transformed to the synchronous dq frame using Clarke/Park transformations. Neglecting iron loss, higher-order saturation effects, and inverter dead time, the standard SPMSM voltage model is [9].

$$u_d = R_s i_d + L_d \frac{di_d}{dt} - \omega_e L_q i_q \tag{5}$$

$$u_q = R_s i_q + L_q \frac{di_q}{dt} + \omega_e \left(L_d i_d + \psi_f \right) \tag{6}$$

The electromagnetic torque and mechanical motion equations are respectively

$$T_e = 1.5p[\psi_f i_q + (L_d - L_q) i_d i_q] \tag{7}$$

$$J\frac{d\omega_m}{dt} = T_e - T_L - B\omega_m \tag{8}$$

$$T_e = 1.5p\left[\psi_f i_q + \left(L_d - L_q\right) i_d i_q\right] \tag{9}$$

$$J\frac{d\omega_m}{dt} = T_e - T_L - B\omega_m \tag{10}$$

For surface-mount PMSM, the difference between Ld and Lq is small, and the reluctance torque term is relatively weak. After using id=0 control, the torque is mainly generated by the q-axis current, and the torque equation can be simplified as

$$T_e \approx 1.5p\psi_f i_q = K_t i_q \tag{11}$$

With p=2 and ψf=0.32 Wb, Kt≈0.96 N·m/A and the 9.55 N·m rated torque requires iqN≈9.95 A. This value checks the consistency of q-axis current and torque after loading.

3.2 Current Loop, Velocity Loop and Local Gain Sweep

After dq decoupling compensation, the single-axis current object can be approximated as a first-order link determined by the stator resistance and synchronous inductance, see Table 4.

$$G_i(s) = \frac{1}{L_s s + R_s} \tag{12}$$

Table 4 Parameters of Three PI Schemes

plan	Kpi	Kii	Kpw	Kiw	Description
Manual PI baseline	20	6000	0.35	60	Empirical gains for stable operation
Parameter matching PI	41	14250	0.75	150	Matched by Rs, Ls, J, Kt
Matched PI + local optimization	49.2	17100	1.05	210	Best result within the tested gain grid

The current loop sampling period is Tsi=100 μs. When performing engineering tuning based on inductance, sampling period and electrical time constant, the proportional coefficient and integral coefficient are calculated according to Equation (13).

$$K_{pi} = \frac{0.5L_s}{T_{si}}, \quad K_{ii} = \frac{K_{pi}R_s}{L_s} \tag{13}$$

With Tsi=100 μs, Ls=8.2 mH, and Rs=2.85 Ω, Equation (13) gives Kpi≈41 and Kii≈14250 using a 0.5 engineering correction. For Kt/(Js+B) and Tsw=1 ms, Kpw=0.75 and Kiw=150.
The local scan retains the controller structure, scaling speed-loop gains by 0.6–1.4 and current-loop gains by 0.8–1.2.

$$F = M_p + 0.01\Delta n_{\text{load}} + 100t_{\text{rec}} + 2e_{iq} \tag{14}$$

Equation (14) ranks combinations using overshoot, speed drop, recovery time, and q-axis current error; the selected gains are locally, not globally, optimal.

4 SIMULINK AVERAGE MODEL AND EVALUATION INDICATORS

A three-branch Simulink average-value model compares the PI schemes with identical motor, load, sampling, and limiting settings, see Figure 6. The 20 μs simulation step, 100 μs current-loop sampling, 1 ms speed-loop sampling, and linear-region SVPWM support low-frequency dynamic comparison, not device-level switching analysis [10].

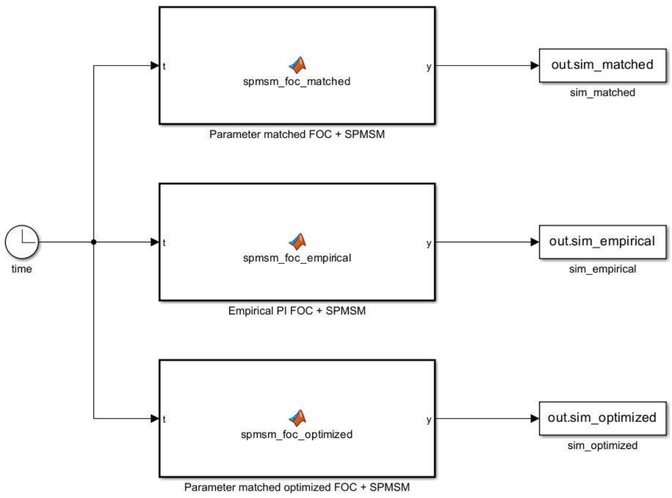

Figure 6 Simulink Top-level Model for Parallel Comparison of Three Solutions

The speed reference ramps to 1500 r/min by 0.12 s; 9.55 N·m is applied at 0.2 s and removed at 0.4 s.
Startup and recovery are measured within a sustained ±2% speed band, and Equation (15) defines load drop and q-axis tracking error.

$$\begin{cases} \Delta n_{\text{load}} = n_{\text{ref}} - \min n(t), t \in [0.2, 0.4)\text{s} \\ e_{iq} = \sqrt{\text{mean}\left[\left(i_q - i_q^*\right)^2\right]} \end{cases} \tag{15}$$

5 RESULTS AND DISCUSSION

5.1 Comparison of Starting and Load Disturbance under Nominal Operating Conditions

Figure 7 compares speed responses under identical conditions. All schemes track the 0–0.12 s ramp. After the 9.55 N·m load step at 0.2 s, speed drops are 191.40, 111.11, and 95.14 r/min for the manual, matched, and locally optimized PI schemes, respectively. Parameter matching improves plant–controller consistency, and local refinement further accelerates recovery.

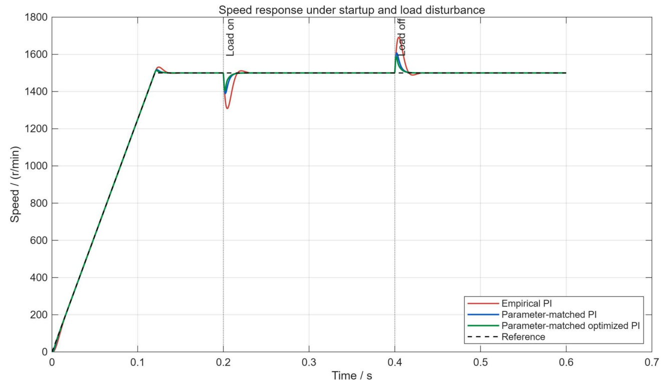

Figure 7 Comparison of Speed Response of Three PI Schemes

Figure 8 shows that each controller increases electromagnetic torque after loading. The manual PI builds compensation more slowly, whereas the matched and optimized schemes establish q-axis torque current faster. Further gain increases remain constrained by voltage limits, overshoot, and current-tracking error.

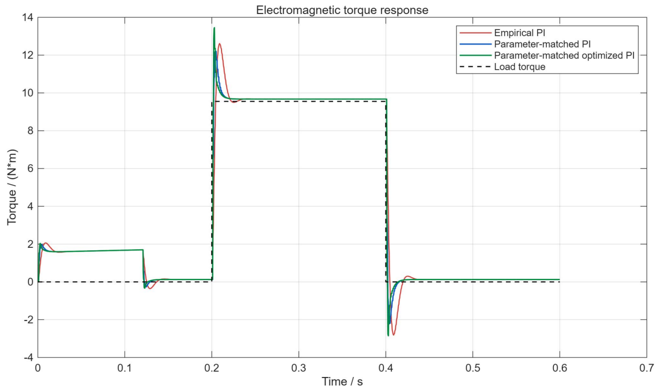

Figure 8 Comparison of Electromagnetic Torque Response of Three PI Schemes

Figure 9 confirms id≈0 and an iq rise to about 10 A after loading, close to the calculated rated-torque requirement iqN≈9.95 A. This agreement links the torque equation, load setting, and simulated current response.

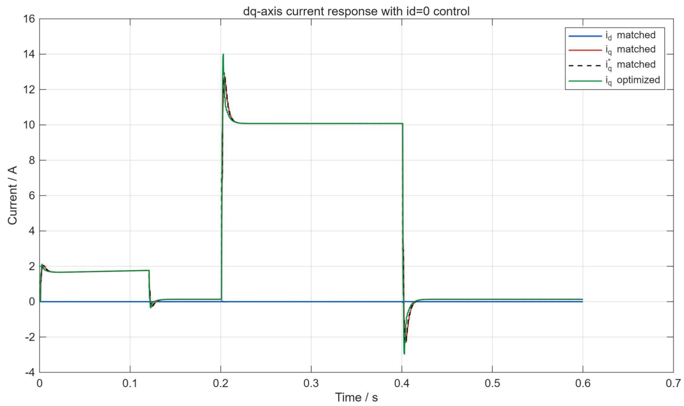

Figure 9 dq-axis Current Response under Parameter Matching PI

Table 5 quantifies Figures 7–9. Relative to manual tuning, parameter matching reduces load speed drop by 41.9%, recovery time by 43.4%, and iq error from 0.00695 to 0.00020 A. Local optimization yields reductions of 50.3% and 58.1% in speed drop and recovery time, respectively. These results demonstrate improved disturbance rejection within the tested conditions, not universal stability.

Table 5 Comparison of Performance Indicators under Nominal Operating Conditions

plan	Start time/s	Maximum overshoot/%	Load drop/(r/min)	Recovery time/s	iq tracking error/A
Manual PI baseline	0.10584	2.092	191.40	0.01354	0.00695
Parameter matching PI	0.09760	1.176	111.11	0.00766	0.00020

plan	Start time/s	Maximum overshoot/%	Load drop/(r/min)	Recovery time/s	iq tracking error/A
Parameter matching + optimization PI	0.09760	0.92955	95.145	0.00568	0.00016

5.2 Parameter Perturbation Tolerance and Local Gain Sweep

Figure 10 and Table 6 show that the matched PI maintains smaller speed drops and recovery times under the specified variations in Rs, Ldq, ψf, and J. Increasing J by 50% reduces the instantaneous speed drop but lengthens recovery because greater inertia slows mechanical response. The combined case is treated as a parameter combination rather than a strict worst case.

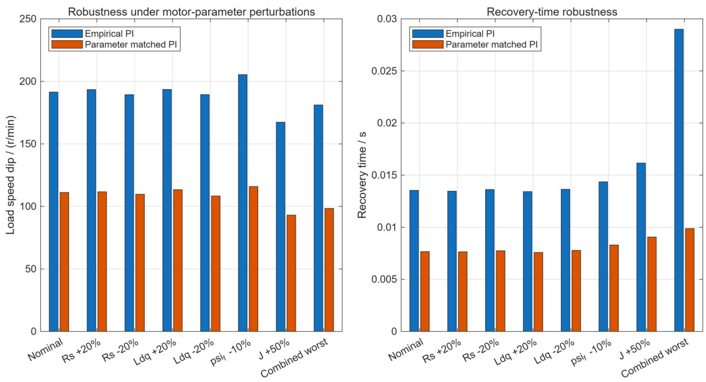

Figure 10 Comparison of Load Drop and Recovery Time under Parameter Disturbance

Table 6 Parameter Perturbation Tolerance Results

Disturbance conditions	Manually adjust PI drop	Matched PI drop	Manual PI recovery/s	Matched PI recovery/s
Nominal operating conditions	191.40	111.11	0.01354	0.00766
Rs +20%	193.43	111.69	0.01346	0.00764
Rs -20%	189.35	109.70	0.01362	0.00774
Ldq +20%	193.54	113.37	0.01342	0.00758
Ldq -20%	189.42	108.33	0.01364	0.00778
ψf -10%	205.39	115.90	0.01436	0.00830
J +50%	167.33	93.02	0.01616	0.00906
Combinatorial perturbation	181.12	98.42	0.02900	0.00988

Figure 11 identifies the best score in the tested grid at speed-loop scaling 1.4 and current-loop scaling 1.2, giving Kpi=49.2, Kii=17100, Kpw=1.05, and Kiw=210. Moderate gain increases therefore improve load response within this scan and average-value model, but the result is not a global optimum.

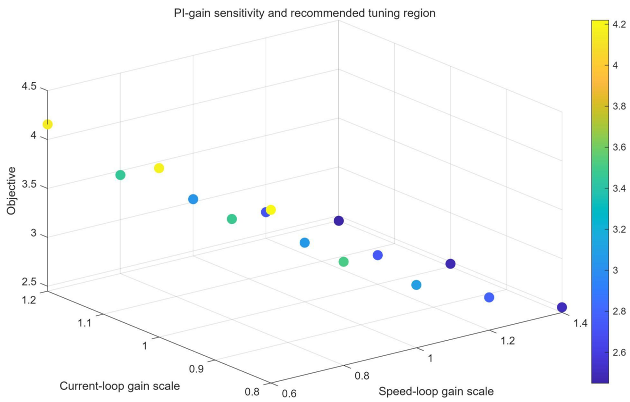

Figure 11 PI Gain Local Scan Results

6 CONCLUSION

This study develops a joint RMxprt/Maxwell–Simulink workflow for a 1.5 kW, 4-pole, 24-slot SPMSM. Finite-element analysis checks rated and electromagnetic consistency, while the discrete dq model compares controllers under identical conditions.

Parameter matching reduces rated-load speed drop from 191.40 to 111.11 r/min and recovery time from 0.01354 to 0.00766 s; local refinement reaches 95.14 r/min and 0.00568 s. Current and perturbation results support the advantage within the tested range.

The model omits switching, dead time, saturation, temperature drift, hardware validation, and multi-motor testing. Future work should import operating-point-dependent finite-element maps and conduct hardware-in-the-loop and prototype experiments.

COMPETING INTERESTS

The authors have no relevant financial or non-financial interests to disclose.

REFERENCES

[1] Monadi M, Nabipour M, Akbari-Behbahani F, et al. Speed control techniques for permanent magnet synchronous motors in electric vehicle applications toward sustainable energy mobility: A review. IEEE Access, 2024, 12: 119615-119632.

[2] Bae Y, Kim J M. Real-time PI gain auto-tuning for SPMSM drives based on time-domain response characteristics. Energies, 2025, 18(18): 4899.

[3] Shi S, Guo L, Chang Z, et al. Current controller based on active disturbance rejection control with parameter identification for PMSM servo systems. IEEE Access, 2023, 11: 46882-46891.

[4] Zhou S, Wang D, Du M, et al. Double update intelligent strategy for permanent magnet synchronous motor parameter identification. Computers, Materials & Continua, 2023, 74(2): 3391-3404.

[5] Liu H, Niu W, Guo Y. Direct torque control for PMSM based on the RBFNN surrogate model of electromagnetic torque and stator flux linkage. Control Engineering Practice, 2024, 148: 105943.

[6] Xiao F, Chen Z, Chen Y, et al. A finite control set model predictive direct speed controller for PMSM application with improved parameter robustness. International Journal of Electrical Power & Energy Systems, 2022, 143: 108509.

[7] Wang L, Zhang S, Zhang C, et al. An improved deadbeat predictive current control based on parameter identification for PMSM. IEEE Transactions on Transportation Electrification, 2024, 10(2): 2740-2753.

[8] Li X, Zhang S, Cui X, et al. Novel deadbeat predictive current control for PMSM with parameter updating scheme. IEEE Journal of Emerging and Selected Topics in Power Electronics, 2022, 10(2): 2065-2074.

[9] Pillay P, Krishnan R. Modeling, simulation, and analysis of permanent-magnet motor drives, part I: The permanent-magnet synchronous motor drive. IEEE Transactions on Industry Applications, 1989, 25(2): 265-273.

[10] Holtz J. Pulsewidth modulation for electronic power conversion. Proceedings of the IEEE, 1994, 82(8): 1194-1214.